
Article:
Rudden, I., Li, G.-J. orcid.org/0000-0002-5956-4033, Kana, D.K. et al. (4 more authors) (2024) Space harmonic cancellation in a dual three-phase SPM machine with star-delta windings. IEEE Transactions on Energy Conversion, 39 (1). pp. 457-468. ISSN 0885-8969

https://doi.org/10.1109/TEC.2023.3292406

Space Harmonic Cancellation in a Dual Three-Phase SPM Machine with Star-Delta Windings

I. A. Rudden[1], G. J. Li[1], *Senior Member, IEEE*, D. K. Kana Padinharu[1], Z. Q. Zhu[1], *Fellow, IEEE*, A. Duke[2], R. Clark[2], and A. Thomas[2]
1, Department of Electronic and Electrical Engineering, The University of Sheffield, Sheffield, UK
2, Siemens Gamesa Renewable Energy Limited, North Campus, Broad Lane, Sheffield, UK
g.li@sheffield.ac.uk.

***Abstract*—This paper proposes a dual 3-phase SPM machine with star-delta windings. The machine is based on the widely adopted 12s/10p configuration and employs a number of methods to suppress the two largest core loss causing MMF harmonics. Firstly, stator shifting is used to reduce the 7th order harmonic, which is then completely suppressed through the use of a second 3-phase converter operating at a 15° phase shift with regard to the first one. Secondly, each of the winding sets employs 3-phase star-delta winding that are able to completely cancel the 1st order MMF harmonic. Additionally, these methods increase the amplitude of the torque producing harmonic and so yield a machine with better torque performance than a conventional 3-phase machine. Analytical modelling is used to demonstrate the cumulative impact on winding MMF harmonics. FEA is then used to validate the analytical predictions and to investigate other machine performance. The proposed machine demonstrates comparable average torque and efficiency to a 12-slot dual 3-phase machine, but offers a substantial reduction in torque ripple and PM eddy current losses. This helps improve the machine performance and reduce the risk of thermal demagnetization. A prototype machine has been manufactured and EMF and static torque measurements validate the expected performance of the proposed machine.**

Keywords— Dual 3-phase, fractional-slot concentrated windings, star-delta, stator shifting.

I. Introduction

It has been demonstrated that fractional-slot concentrated windings (FSCW) offer several substantial advantages over conventional integer-slot distributed windings [1]. If used with permanent magnets they can achieve similar power densities and efficiencies to integer slot machines, yet have shorter end-windings (so reduced copper losses), higher slot-fill factors, easier manufacturability (particularly if a segmented stator is used), higher fault tolerance, and lower cogging torque [2],[3],[4],[5]. However, the downside of FSCW is the presence of many sub and super space harmonics that rotate asynchronously with the rotor, and thus induce unwanted eddy current losses in the rotor core and PMs [6],[7],[8]. This is even more prominent in machines with single-layer windings as opposed to double-layer windings [9]. A large amount of work has been done developing models to understand and mitigate these losses [5],[10],[11],[12] as the rotor is harder to cool than the stator and excessive temperatures within the PMs due to additional eddy current losses can lead to thermal demagnetization [13],[14]. Additionally, the interaction between these asynchronous field components and the rotor can lead to unwanted noise and vibration in the system [15]. In a lot of applications, it is desired for the torque ripple to be less than 1% of the average torque. This is harder to achieve using concentrated windings compared with distributed ones.

Many methods exist to mitigate unwanted harmonics, including the common practice such as adding additional winding layers [16]. By moving beyond double-layer windings, the machine efficiency can be improved by reducing the winding factor of the most dominant subharmonic. Stator shifting can also be employed to cancel unwanted harmonics[17], [18], [19]. The principle of stator shifting is to essentially superimpose two stator windings into one machine. This works by doubling the number of slots, with the second winding set being placed in between the slots of the first winding set. The winding layouts are the same, but the second winding set is shifted by α mechanical degrees– α being determined by the selected harmonic to be minimized. The result is a pseudo-distributed winding, as each coil now spans two stator slots. Although this is a step away from concentrated windings, the benefit of harmonic minimization often outweighs the increased machine complexity. Multiphase machines are also a good strategy for mitigating unwanted harmonics [20], [21], [22], [23], [24]. This works by introducing more than 3-phase such that each phase is at an optimum phase shift to minimize parasitic harmonics. Such methods can also be applied to a dual 3-phase system [25], [26]. All these methods demonstrate that through the addition of more phases, more harmonics can be reduced but at a price of increasing the complexity through either increasing the number of legs in the converter for multiphase machines, or through the introduction of an additional converter for dual 3-phase machines. However, additional converters (or legs) also provide higher fault tolerance. In the event of a converter failure the machine can continue to operate at a reduced load by using the remaining healthy converter (or legs). This has made dual 3-phase machines a particularly attractive option due to their improved performance over conventional 3-phase machines in addition to the redundancy a second converter adds to system reliability [25]. Due to the advantage of dual 3-phase machines in terms of improving machine performance compared to a conventional 3-phase machine, a novel 3-phase machines with star-delta windings has been proposed to mimic the behavior of a dual 3-phase machine in [27]. This is achieved as a phase shift of 30° is present between the star windings and delta windings. Similarly, a star-delta machine was proposed in [28] that offers excellent harmonic suppression. However, these approaches lose the fault tolerant capability achieved by adopting two separate converters, and neither achieve 100% cancellation of both a sub and higher order winding MMF space harmonic.

In this paper, to combine the merits of stator shifting and star-delta windings as well as dual 3-phase systems, a dual 3-phase 24s/10p machine with star-delta windings is proposed that can reduce rotor and PM eddy current losses through cancellation of the dominant sub and super space harmonics. The proposed machine will be compared against five other machines, i.e., a conventional 3-phase 12s/10p machine, a dual 3-phase 12s/10p machine [27], a conventional 3-phase 24s/10p machine [19], a dual 3-phase 24s/10p machine and a 3-phase 24s/10p machine with star-delta windings [28].

These six machines will be compared in terms of armature MMF, torque performance, losses and efficiency to build a complete picture regarding the advantages of the proposed design. It is found that the proposed design shows similar torque performance and efficiency to the conventional 12s/10p dual 3-phase counterpart but offers a significant reduction in torque ripple (<1% of average torque). This is in addition to the greatly reduced PM eddy current losses and so reduced risk of thermal demagnetization.

II. Winding Theory

A. Star-Delta Windings

The fundamental principle behind employing star-delta windings is to exploit the inherent phase shift between currents in the two winding sets. In an n-phase system the delta winding currents will be shifted by $\pi/2n$ electrical degrees with respect to the star winding currents, so for a 3-phase system this would be 30°. This is achieved by connecting the ends of the star windings to the junctions of the delta windings, and an example of this for a 3-phase system is shown in Fig. 1 (a) and (b). Furthermore, the line voltage of a delta connection is $\sqrt{3}$ times that of a star connection. Fig. 1 (c) shows a phasor diagram of the hybrid connection including phase shift and difference in voltage magnitude between the star and delta windings.

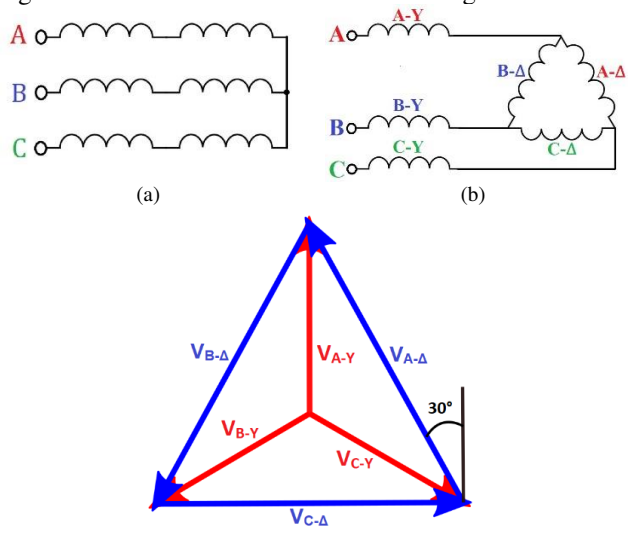

Fig. 1. Winding Structures. (a) conventional winding, (b) star-delta winding and (c) star-delta winding voltage vectors.

In [27] this principle is applied to a 12s/10p machine to simulate the performance of a dual 3-phase machine. By connecting one set of coils in delta connection and the other in star, the introduced phase shift successfully cancels the first subspace harmonic while slightly increasing the amplitude of the working harmonic (5th order). The elimination of the first subharmonic serves to reduce rotor and PM losses, assists in machine saliency, and improves overall efficiency. Additionally, the increase in the working harmonic amplitude increases the torque production and thus improves the electromagnetic performance. However, the difference in phase current magnitude must be accounted for. In the case of a 3-phase machine, the current in the delta windings is $1/\sqrt{3}$ times of that in the star windings. To ensure that the MMF generated by the delta coils is equivalent to the star coils, the number of turns must be multiplied by $\sqrt{3}$ whilst ensuring that the copper volume (and copper loss) of both winding types remains the same.

B. Stator Shifting

The approach of stator shifting is essentially adjusting the winding factors of different machine harmonics. For example, by introducing a second 3-phase winding set with a shift angle α with regard to the first winding set, its unwanted harmonic is added to the same harmonic order of the first winding set. This superposition of harmonics can be explained by plotting the resultant winding factor against shift angle α, as shown in Fig. 2. In the case of a 12s/10p machine the working harmonic is the 5th with the 1st and 7th being loss producing components. It can be seen that if α is properly selected, the 1st or 7th order harmonic can be completely suppressed. However, complete suppression of an unwanted harmonic, such as the 1st, could lead to elimination of the useful harmonic. Therefore, α must be properly selected to reduce the unwanted harmonics with minimum reduction of the working harmonic.

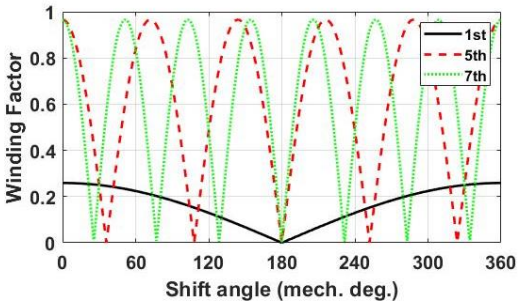

Fig. 2. Winding factor of MMF harmonics *vs* mechanical shift angle α.

In order to maintain equal tooth widths in the machine with stator shifting, a stator shift angle must be equivalent to a multiple of $2\pi/N_s$, where N_s is the number of slots. As the machine with stator shifting will have 24 slots (derived from a conventional 3-phase 12s/10p machine), a multiple of 15 mech. deg. must be selected. It can be seen in Fig. 2 that 75 mech. deg. offers substantial reduction in the 7th order harmonic, with only a minor reduction in the winding factor of the torque producing harmonic (5th order). A 75 mech. deg. phase shift between the two windings set is equivalent to a 375 elec. deg. (or 15 elec. deg.) phase shift for a 10-pole machine. As a result, if the 3-phase currents of the second converter have a 15 elec. deg. phase shift compared to the first converter, complete cancellation of the 7th order harmonic can be achieved while maintaining the fundamental.

C. Winding Layout

It has been proven in literature that the implementation of star-delta windings can completely suppress the 1st order harmonic in a 12s/10p machine [27]. Additionally, the stator shifting + use of a second converter should completely cancel the 7th order harmonic. Thus, this paper proposes a new method that adopts a combination of star-delta windings and stator shifting with a second converter, which should yield complete cancellation of the 1st and 7th order unwanted MMF harmonics. To validate this, in addition to two 12s/10p machines (conventional 3-phase and dual 3-phase), four 24s/10p machines as shown in Fig. 3 will also be investigated. A 3-phase 24s/10p machine [Fig. 3 (a)] will be used as a baseline to show the efficacy of the proposed harmonic suppression through stator shifting. Fig. 3 (b) shows a dual 3-phase machine that should achieve complete cancellation of the 7th order harmonic provided the second converter is operating at the required 15 elec. deg. phase shift with regard to the first converter. Fig. 3 (c) shows a 3-phase star-delta machine that should completely cancel the 1st order

subharmonic, and finally Fig. 3 (d) shows the proposed dual 3-phase machine with star-delta windings that should benefit from the cumulative effect of stator shifting, dual 3-phases and star-delta windings. In addition, the winding connections and the coil EMF vector diagram of the proposed dual 3-phase machine with star-delta windings can be seen in Fig. 4. The original topologies are based on the machines investigated in [29] and the machine specifications are given in TABLE I.

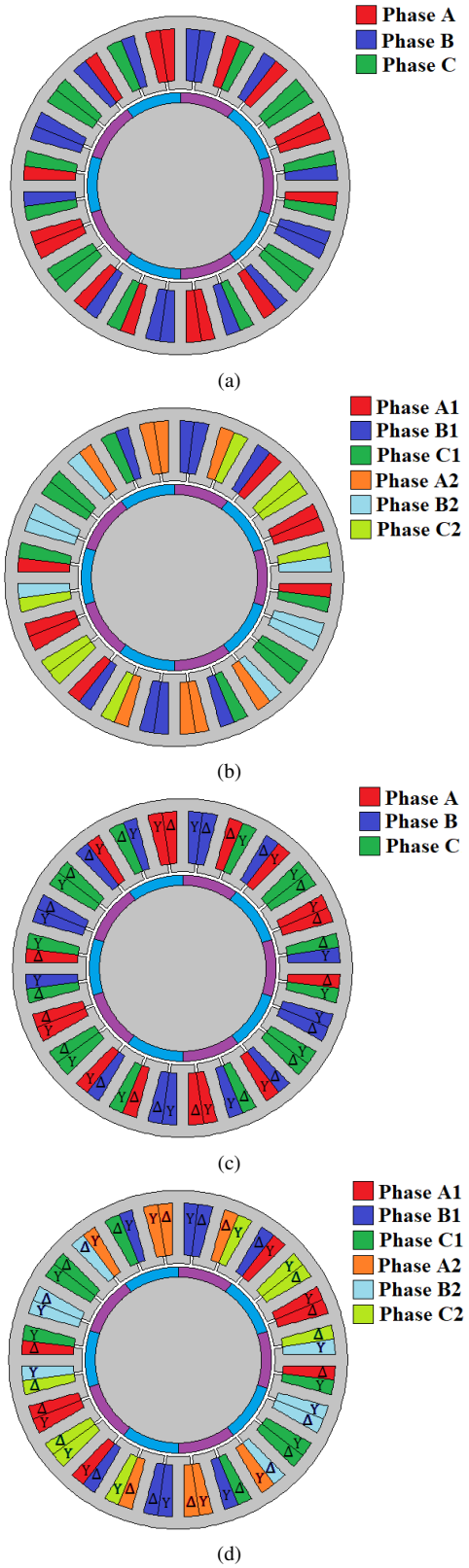

Fig. 3. Machine winding layouts for 24s/10p machines. (a) 3-phase, (b) dual 3-phase, (c) 3-phase star-delta, and (d) dual 3-phase star-delta winding layouts. Δ is for delta winding and Y is for star winding.

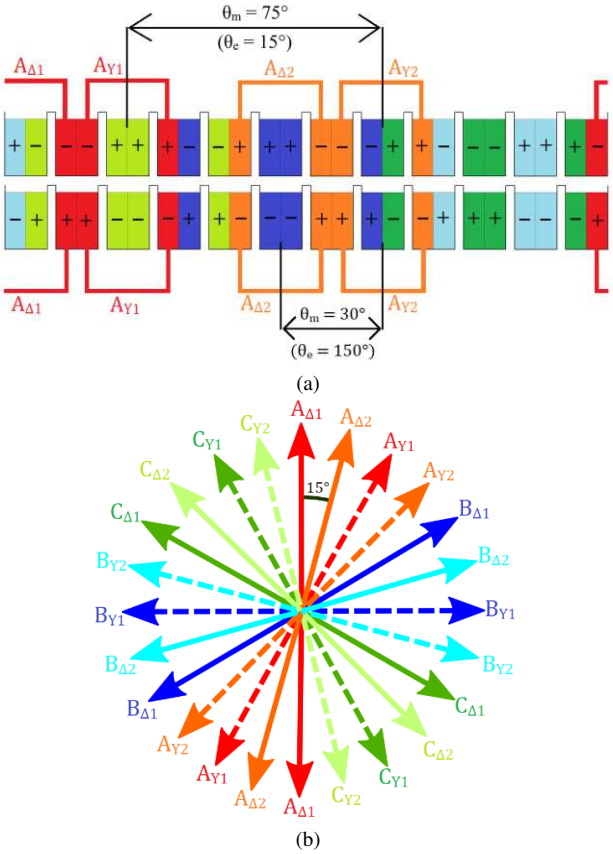

Fig. 4. (a) Winding schematic (read left to right across the top row then left to right across the bottom row) and (b) phasor diagram for a 24s/10p dual 3-phase machine with star-delta windings.

TABLE I PROPOSED MACHINE SPECIFICATIONS

Slot number	12/24	Stack length (mm)	50
Pole number	10	Air-gap length (mm)	1
Rated current (A_{rms})	7.34	Tooth width (mm)	7/3.5
Rated speed (RPM)	400	Tooth height (mm)	2.5
Turns per phase	132/66	Stator yoke height (mm)	3.7
Stator outer radius (mm)	50	Magnet thickness (mm)	3
Rotor outer radius (mm)	27.5	Magnet remanence (T)	1.24

III. Analytical Modelling

A. Calculation of Winding MMF

It has been shown in [27] that the turn functions of phases A1 and A2 in the 12s/10p dual 3-phase machine can be expressed as

$$\begin{cases} N_{A1}(\theta) = \sum_{k=1,3,\dots}^{\infty} \frac{4N_{c1}}{k\pi} \sin\left(\frac{k\pi}{12}\right) \sin(k\theta) \\ N_{A2}(\theta) = -\sum_{k=1,3,\dots}^{\infty} \frac{4N_{c2}}{k\pi} \sin\left(\frac{k\pi}{12}\right) \sin\left(k\left(\theta - \frac{\pi}{6}\right)\right) \end{cases} \quad (1)$$

where N_{c1} and N_{c2} are the number of turns per coil for phases A1 and A2 respectively, θ is the angular position, and $\pi/6$ (elec. deg.) accounts for the shift in space of the second winding set with respect to the first. Each winding set is fed by balanced three phase currents, with the second set converter operating at a 30 elec. deg. phase shift to the first. This results in the MMF produced by each winding set being given by,

$$F_{A1}(\theta, t) = \sum_{k=1,-5,7,\dots}^{\infty} \frac{6N_{c1}I_m}{k\pi} \sin\left(\frac{k\pi}{12}\right) \cos(k\theta - \omega t)\cos(\omega t) \quad (2)$$

$$F_{A2}(\theta,t) = -\sum_{k=1,-5,7,\ldots}^{\infty} \frac{6N_{c2}I_m}{k\pi}\sin\left(\frac{k\pi}{12}\right)\cos\left(k\left(\theta-\frac{\pi}{6}\right)+\frac{\pi}{6}-\omega t\right)\cos(\omega t) \quad (3)$$

These equations also result from employing a star-delta winding connection, as the currents in the star winding are shifted by 30 elec. deg. with respect to the delta winding. In this case, the phase current would be $\sqrt{3}$ times greater in the star connected coils, and so the number of turns in the delta winding must be $\sqrt{3}$ higher.

For the 24s/10p machines, the second winding set is shifted by 150 mech. deg., the third by 375 mech. deg. (or 15 elec. deg.), and fourth by 525 mech. deg. (or 165 elec. deg.) The winding equations are fundamentally the same for all four 24s/10p machines, the only difference is the varying phase shifts that come about from either the second converter or the use of star-delta windings, as well as the number of turns in the star or delta wound coils. For the conventional and dual 3-phase machines $N_{c1} = N_{c2}$, but in the star-delta winding machines $N_{c1} = \sqrt{3}\,N_{c2}$ to account for the reduced current in the delta windings. The combination of the mechanical shift between winding sets and the phase shifts provided by either a second converter or star-delta windings provides the following set of winding function equations for Phase A,

$$F_{A1}(\theta,t) = \sum_{k=1,-5,7,\ldots}^{\infty} \frac{6N_{c1}I_m}{k\pi}\sin\left(\frac{k\pi}{12}\right)\cos(k\theta-\omega t)\cos(\omega t) \quad (4)$$

$$F_{A2}(\theta,t) = -\sum_{k=1,-5,7,\ldots}^{\infty} \frac{6N_{c2}I_m}{k\pi}\sin\left(\frac{k\pi}{12}\right)\cos\left(k\left(\theta-\frac{\pi}{6}\right)+\theta_s-\omega t\right)\cos(\omega t) \quad (5)$$

$$F_{A3}(\theta,t) = \sum_{k=1,-5,7,\ldots}^{\infty} \frac{6N_{c1}I_m}{k\pi}\sin\left(\frac{k\pi}{12}\right)\cos\left(k\left(\theta-\frac{5\pi}{12}\right)+\theta_c-\omega t\right)\cos(\omega t) \quad (6)$$

$$F_{A4}(\theta,t) = -\sum_{k=1,-5,7,\ldots}^{\infty} \frac{6N_{c2}I_m}{k\pi}\sin\left(\frac{k\pi}{12}\right)\cos\left(k\left(\theta-\frac{7\pi}{12}\right)+\theta_s+\theta_c-\omega t\right)\cos(\omega t) \quad (7)$$

where θ_s is the phase shift between the star-delta windings (30 elec. deg.) and θ_c is the phase shift of the second converter with respect to the first converter (15 elec. deg.). It is evident that the equations are the same for all 24s/10p machines, the different results come from values ascribed to either θ_s or θ_c. In the case of the conventional 3-phase machine, both values are set to zero as the windings are connected in star and no second converter is used. In the dual 3-phase machine, θ_c is set to -15 elec. deg. to represent the converter operating at this phase shift. In the 3-phase star-delta machine θ_s is set to 30 elec. deg. to represent the phase shift between star and delta windings. Finally, in the dual 3-phase star-delta machine θ_c and θ_s are set to -15 elec. deg. and 30 elec. deg. respectively.

These equations can be extended to model all three phases (A, B and C), and the combined winding MMFs have been summed up and a comparison amongst all the investigated machines is shown in Fig. 5.

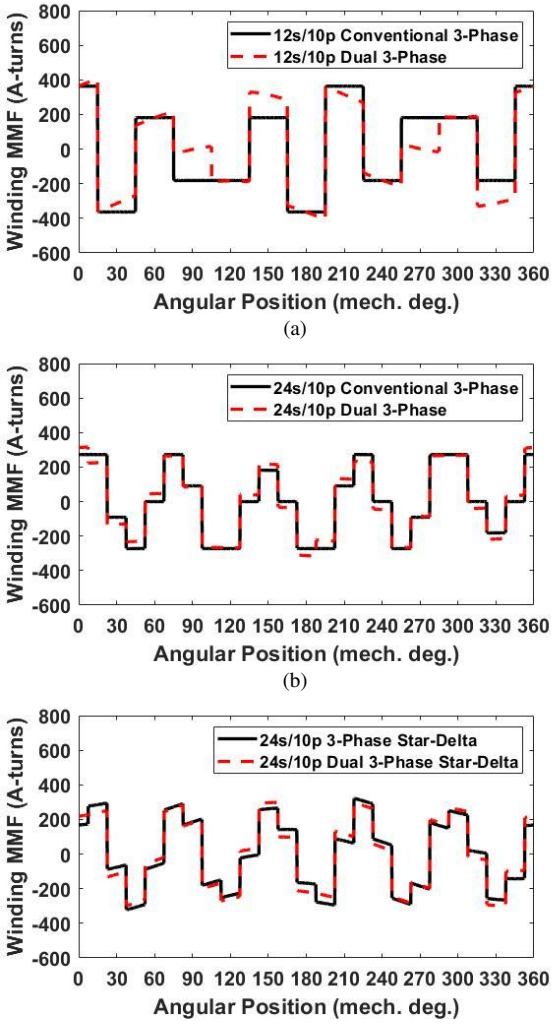

Fig. 5. Winding MMF of each machine. (a) 12s/10p conventional 3-phase and 12s/10p dual 3-phase, (b) 24s/10p conventional 3-phase and 24s/10p dual 3-phase, and (c) 24s/10p star-delta winding and 24s/10p dual star-delta winding.

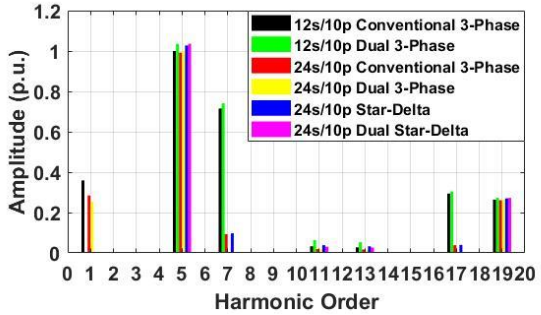

Fig. 6. Comparison of winding MMF harmonics.

Fig. 6 shows the harmonic spectra of each winding MMF. The amplitude is measured in per-unit (p.u.) and the working harmonic of the conventional 12s/10p 3-phase machine is used as reference. The different winding structures each exhibits different harmonic cancellation properties. As expected, the dual 3-phase 12-slot machine completely cancels the first subharmonic in addition to a slight increase in the working harmonic (5th order). The 24-slot machines each exhibits a strong reduction in the unwanted 7th order harmonic owing to the stator shifting, with the dual 3-phase 24-slot machine showing complete cancellation of the 7th order space harmonic. Additionally, the 24-slot machine employing star-delta windings shows complete cancellation of the 1st order sub-space harmonic much like its 12-slot

counterpart. Finally, the cumulative effect of both the star-delta windings and a second converter working at a 15 elec. deg. phase shift offers complete cancellation of both the 1st order sub-space harmonic and 7th order super harmonic. Similarly, each winding structure influences the amplitude of the working harmonic, with the dual 3-phase star-delta winding boasting the largest increase as shown in Table II. The combination of parasitic harmonic cancellation and increase in the working harmonic amplitude suggests that the dual 3-phase 24s/10p machine with star-delta windings should offer better torque performance than the 12s/10p dual 3-phase machine in addition to reducing rotor and PM losses.

TABLE II IMPACT OF WINDING STRUCTURE ON WORKING HARMONIC AMPLITUDE WITH REFERENCE TO CONVENTIONAL 3-PHASE 12S/10P MCHINE

Winding Type	Increase in working harmonic
12s/10p conventional 3-phase	0
12s/10p dual 3-phase	+3.5%
24s/10p conventional 3-phase	-0.8%
24s/10p dual 3-phase	+0.1%
24s/10p 3-phase star-delta	+2.7%
24s/10p dual 3-phase star-delta	+3.6%

B. Calculation of Air-Gap Permeance

The air-gap permeance of the machines is also modelled analytically using a similar method to the one developed in [30]. In [30], three different methods of air-gap permeance calculation were investigated, i.e. sinusoidal shaping, the Weber method and piecewise function. It is demonstrated that for machines with fractional slot concentrated windings and stator tooth tips, the sinusoidal shaping method is simple and can accurately predict the air-gap flux density. Therefore, this method will be used in this paper. The sinusoidal shaping method adopts the principle such that the permeance reaches its maximum value where there are tooth tips, and then decreases to its minimum value at the center of each stator slot in a sinusoidal manner. To begin the approximation method, two geometric constants (u and β) derived in [30] and based on the slot geometry must be determined using

$$u = \frac{\tau_s}{2l_g} + \sqrt{1 + (\frac{\tau_s}{2l_g})^2} \tag{8}$$

$$\beta = \frac{1 + u^2 - 2u}{2(1 + u^2)} \tag{9}$$

where τ_s is the width of a stator tooth, and l_g is the mechanical clearance (or air-gap length) in mm. These geometric constants can be used to calculate the maximum and minimum values of air-gap permeance as shown by,

$$P_{max} = \frac{1}{l_g} \tag{10}$$

$$P_{min} = \frac{1 - 2\beta}{l_g} \tag{11}$$

Using these equations, the relative air-gap permeance around the circumference of the machine can be calculated using (12), where α_t is the mechanical angle of a tooth tip. Multiplying the relative air-gap permeance by the permeability of free space gives the machine air-gap permeability. To verify these analytical calculations, the air-gap permeance was extracted from the FEA models of both machines. This was achieved by calculating the open-circuit flux density (produced by the PMs) for the machines with and without slots, and then dividing the flux density with slots by the one without slots. This gives a relative air-gap permeance of the machine with slots. After multiplying by the permeability of free space, this permeance is mapped onto the analytical model, as shown in Fig. 7

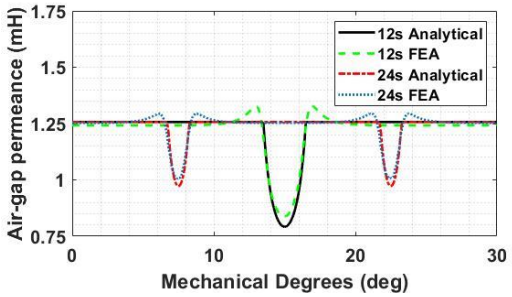

Fig. 7. Air-gap permeance of both machines extracted from FEA compared with analytical results.

There is good agreement between the analytically calculated air-gap permeance and that extracted from the FEA models. However, there is a slight discrepancy caused by slot leakage and the fringing flux between stator teeth that is not accounted for in the analytical model, but for the purposes of this investigation the model is accurate enough. Multiplying the winding MMF calculated in the previous section by this air-gap permeance gives the resulting air-gap flux density produced by armature currents. This allows for comparison of air-gap flux density with the FEA results, as detailed in the following section.

C. Air-gap Flux Density due to Winding MMF

FEA modelling of the air-gap flux density has also been carried out. The six investigated machines were modelled in OPERA 2D with the permanent magnets removed and windings sinusoidally excited. The sinusoidal excitation of the windings produced an armature field in the air-gap which has been compared against the analytically calculated results, as shown in Fig. 8.

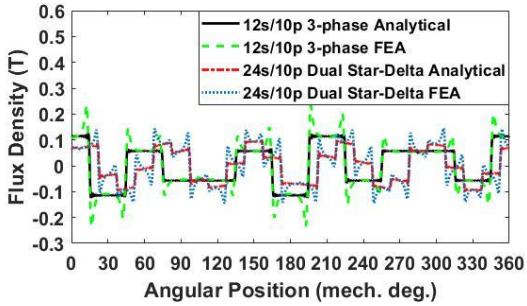

Fig. 8. Comparison of analytical and FEA flux densities.

There is a reasonable match between the FEA and analytically calculated flux density. However, as the analytical model does not incorporate slot leakage or account for the fringing of flux at the stator tooth tips, there are spikes of increased flux density at every tooth tip edge. To remove this effect and thus verify the accuracy of the model, the PMs were replaced with iron such that the effective air-gap length for the armature winding MMF was reduced to 1mm.

$$P'(\theta) = \begin{cases} P_{max} & , \quad 0 \le \theta \le \frac{\alpha_t}{2} \\ \left(\frac{P_{max} + P_{min}}{2}\right) + \left(\frac{P_{max} - P_{min}}{2}\right)\cos\left[\frac{2\pi}{\alpha_s}\left(\theta - \frac{\alpha_t}{2}\right)\right] & , \quad \frac{\alpha_t}{2} \le \theta \le \frac{\alpha_t}{2} + \alpha_s \\ P_{max} & , \quad \alpha_s + \frac{\alpha_t}{2} \le \theta < \theta_s \end{cases} \tag{12}$$

This greatly decreased the impact of fringing flux and slot leakage, and the FEA results are once again compared against the analytical results, as shown in Fig. 9.

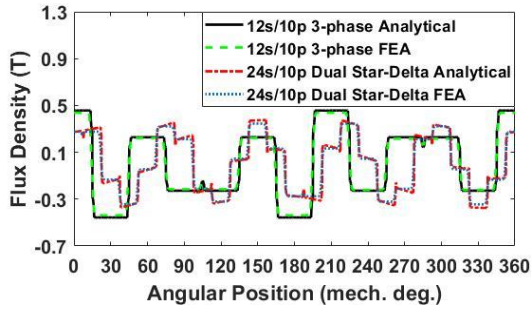

Fig. 9. Comparison of analytical and FEA flux densities.

As can be seen, there is now good agreement between flux density calculated by the analytical model and obtained from FE simulated machines. Additionally, the relative harmonic spectra of both analytical and FE air-gap flux densities show good agreement, as shown in Fig. 10.

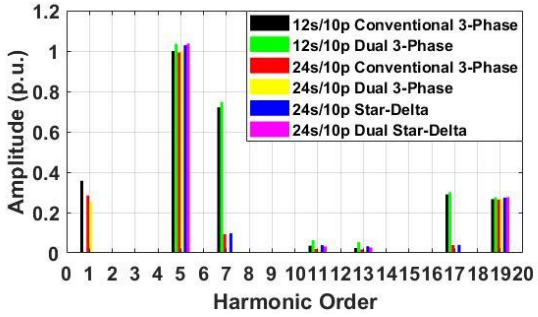

(a)

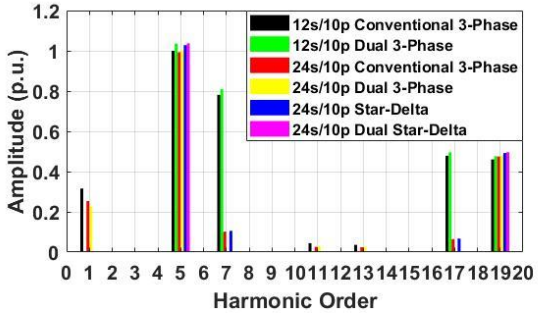

(b)

Fig. 10. Comparison of air-gap flux density harmonics. (a) Analytical and (b) FE results.

TABLE III COMPARISON OF INCREASE IN WORKING HARMONIC AMPLITUDE WITH REFERENCE TO THE CONVENTIONAL 12s/10p 3-PHASE

Winding Type	Analytical	FEA
12s/10p conventional 3-phase	0	0
12s/10p dual 3-phase	+3.5%	+3.6%
24s/10p conventional 3-phase	-0.67%	-0.7%
24s/10p dual 3-phase	+0.02%	+0.2%
24s/10p 3-phase star-delta	+2.8%	+2.8%
24s/10p dual 3-phase star-delta	+3.7%	+3.7%

Both the analytical and FE air-gap flux densities show that the dual 3-phase machine with star-delta windings successfully eliminates both the 1st order subharmonic and 7th order super harmonic. Additionally, both harmonic spectra show good agreement in the impact of each winding structure on the working harmonic amplitude, as shown in Table III.

It can be seen that the 12s/10p dual 3-phase machine increases the amplitude of the working harmonic by the expected 3.5% over the 12s/10p conventional machine. The baseline 24s/10p machine shows a reduction in the working harmonic of about 0.7% with reference to the 12s/10p conventional machine. However, by employing a second converter operating at a 15 elec. deg. phase shift this 0.7% decrease is brought up to a 0.2% increase over the 12s/10p baseline (based on FE results). Similarly, by employing star-delta windings in the 24s/10p machine the relative change in the working harmonic goes from -0.7% to +2.8%. Thus, when the star-delta windings are used in conjunction with a second converter operating at a 15 elec. deg. phase shift the cumulative effect increases the working harmonic by 3.7% over the conventional 12s/10p machine.

D. Torque Performance

In addition to the previous analyses about the air-gap flux density produced by armature currents, the on-load torque has also been investigated. To simplify the analysis, the torque performance will be evaluated using FEA. The six machines were supplied with rated current and their on-load torques are shown in Fig. 11, with a direct comparison given in Table IV.

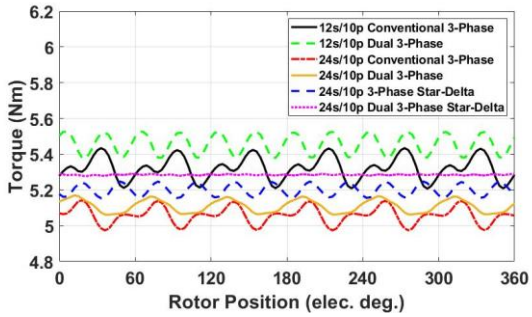

Fig. 11. Torque performance of initial machines.

TABLE IV DIRECT COMPARISON OF TORQUE PERFORMANCE

Winding Type	Average Torque (Nm)	Torque Ripple (Nm)
12s/10p 3-phase	5.32	0.237 *(4.27%)*
12s/10p dual 3-phase	5.46 **(+2.53%)**	0.149 *(2.72%)*
24s/10p 3-phase	5.06 **(-4.94%)**	0.168 *(3.31%)*
24s/10p dual 3-phase	5.11 **(-3.99%)**	0.109 *(2.13%)*
24s/10p 3-phase star-delta	5.20 **(-2.28%)**	0.094 *(1.81%)*
24s/10p dual 3-phase star-delta	5.28 **(-0.69%)**	0.016 *(0.30%)*

As can be seen, the torque performance of the 24-slot machines is less than expected based on the air-gap flux density harmonics. This is attributed to the additional slot leakage of the 24-slot machine, in addition to greater saturation in the stator teeth due to the smaller widths. However, the torque ripple of the 24-slot machines, in particular the dual 3-phase machine with star-delta windings is substantially lower than either of the 12-slot machines. To achieve a fairer comparison, the geometries of the 12-slot and 24-slot machines had to be globally optimized, as detailed in the following section.

IV. Optimised Machine Results

A. Optimisation Process

OPERA's optimization suite was used to optimize the geometries of both the 12-slot and 24-slot conventional 3-phase machines. Other machines with dual 3-phase and star-delta winding structures for each slot/pole number combination will share the same optimized geometries as their conventional 3-phase counterparts. This was decided so that the impact of the winding structure could be investigated for each machine topology entirely independent of other geometrical influences.

During the optimization process, the following values were kept constant: Stator outer diameter, active length, RMS phase current, and PM volume. The aim was to maximize the average torque of both machines without increasing copper losses. This was achieved by constraining the maximum current density in the slots. The full breakdown of optimization parameters can be seen in Table V and includes: split ratio (s), slot-width to tooth-width ratio (β_s), ratio of slot height to stator iron height (h_{sy}), tooth tip to slot opening ratio (t_{ts}), and ratio of tooth tip height to stator tooth width (t_{hw}).

TABLE V OPTIMISATION PARAMETERS

	Optimization Setup
Objective Functions	Maximize Average Torque
Constraints	Maximum Current Density <= 3.368A/mm^2
Model Parameters	0.54 <= s <= 0.66 and 0.4 <= β_s <= 0.6 0.65 <= h_{sy} <= 0.9 and 0.81 <= t_{ts} <= 0.99 0.45 <= t_{hw} <= 0.55

Both optimizations were run until the maximum average torque converged to a result within 0.001Nm, with the 12-slot and 24-slot conventional machines reaching an average torque of 5.41Nm and 5.27Nm respectively. The resulting machine parameters can be seen in Table VI.

TABLE VI OPTIMISATION RESULTS

Universal Parameters		Variable Parameters		
Rated current (A_{rms})	7.34	Slot number	12	24
Rated speed (RPM)	400	Tooth width (mm)	6.45	3.57
Pole number	10	Tooth height (mm)	2.91	1.71
Stator outer radius (mm)	50	Rotor outer radius (mm)	28.2	28.7
Air-gap length (mm)	1	Stator inner radius (mm)	29.2	29.7
Magnet remanence (T)	1.237	Stator yoke height (mm)	3.68	3.43
Turns per phase	132/66	Magnet thickness (mm)	2.92	2.86
Stack length (mm)	50	tooth tip to slot opening ratio	0.81	0.81

B. Torque Performance

With the optimized geometries, the machines were once again operated at rated condition and the on-load torques calculated using FE modelling are shown in Fig. 12. The optimized geometry shows a much better relative performance for the 24-slot machines, likely due to a reduced core saturation. The dual 3-phase machine with star-delta windings shows a comparable average torque to the dual 3-phase 12-slot machine, but also exhibits a substantially reduced torque ripple. A breakdown of these results can be seen in Table VII.

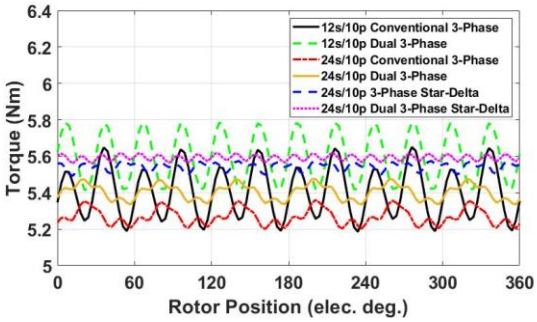

Fig. 12. Torque performance of optimized machines.

TABLE VII DIRECT COMPARISON OF TORQUE PERFORMANCE

Winding Type	Average Torque (Nm)	Torque Ripple (Nm)
12s/10p 3-phase	5.41	0.465 (8.60%)
12s/10p dual 3-phase	5.60 (**+3.58%**)	0.369 (6.59%)
24s/10p 3-phase	5.27 (**-2.56%**)	0.158 (3.01%)
24s/10p dual 3-phase	5.40 (**-0.07%**)	0.140 (2.60%)
24s/10p 3-phase star-delta	5.54 (**+2.54%**)	0.085 (1.52%)
24s/10p dual 3-phase star-delta	5.59 (**+3.44%**)	0.055 (0.99%)

With the optimized geometry the dual 3-phase 24s/10p machine with star-delta windings shows the best overall torque performance, with an average torque just below the 12-slot dual 3-phase machine and a substantially reduced torque ripple. A plot of cogging torque for both the 12-slot and 24-slot machines shows that this large difference in torque ripple is primarily due to the cogging torque, as shown in Fig. 13.

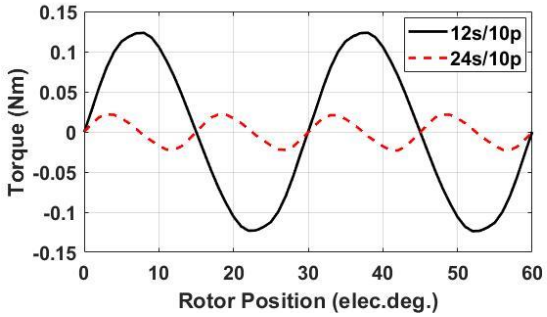

Fig. 13. Cogging torque comparison for 60 electrical degrees.

In addition to the rated torques, the torque performance such as average torque and torque ripple coefficient (peak-to-peak torque over average torque) of the machines across a range of operating conditions have also been investigated, as shown in Fig. 14.

It appears that the optimization process was successful in minimizing the core saturation, as the increase in phase current does not show a sharp drop-off in performance of the 24-slot machines. In fact, from a phase current of 8A the dual 3-phase machine with star-delta windings begins to achieve a higher average torque than the dual 3-phase 12-slot machine, showing a better overload capability. Similarly, a comparison of torque ripple coefficient across a range of phase currents shows that the 24-slot dual 3-phase machine with star-delta windings continues to offer the best performance. For example, at all phase currents the torque ripple of the 12-slot machines remains higher than the 24-slot machines, with the 24-slot dual 3-phase machine with star-delta windings offering the smallest ripple torque coefficient of any machines.

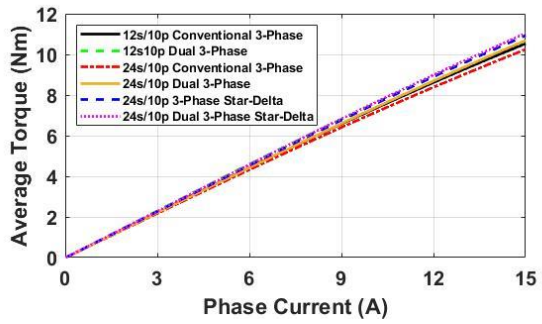

(a)

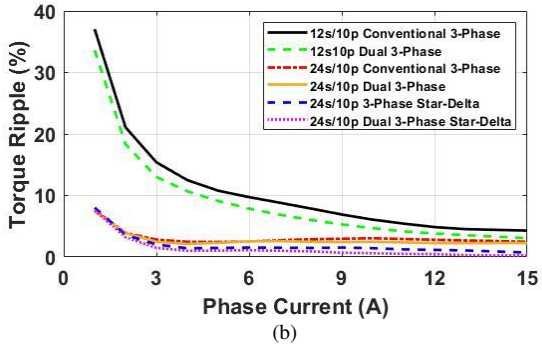

(b)

Fig. 14. (a) Average torque and (b) torque ripple coefficient against phase current.

C. Loss Analysis

The losses of all machines had to be analyzed to ascertain the efficacy of the dual 3-phase star-delta winding in reducing unwanted rotor and PM eddy current losses caused by parasitic harmonics. A script was used to calculate the peak magnetic flux density of different harmonic orders in each mesh element, that could then be used to calculate hysteresis and eddy current losses in the stator and rotor, and eddy current losses in the PMs. To calculate the copper losses, the following equation was used,

$$P_{copper} = N_s N_c^2 \rho \frac{L_w}{S k_b} I_{rms}^2 \qquad (13)$$

where N_s is the number of slots, N_c is the number of conductors per slot, ρ (Ωm) is the resistivity of copper at room temperature, L_w (m) is the sum of both active length and end winding length, S (m^2) is the slot area, k_b is the slot packing factor, and I_{rms} (A) the RMS phase current.

In the 24-slot machines, the number of conductors per slot was half that of the 12-slot machines. In (13) this value is squared, creating a ratio of 1:4 between the 12-slot and 24-slot machines. However, by constraining the maximum allowable current density in the optimization process the total slot area of both machine types should be almost identical, such that the individual slot area of the 24-slot machines should be half that of the 12-slot machines. Thus, it can be seen in (13) that the ratios even out such that the copper losses of both the 12-slot and 24-slot machines are equivalent. In the case of the machines with star-delta windings, the current in the delta windings is reduced by $\sqrt{3}$, but this is offset by increasing the number of conductors in the slot by $\sqrt{3}$ such that the copper losses again remain constant.

It is worth noting that this equation only accounts for the DC copper losses and neglects any AC losses. This does lend an advantage to the 24-slot machine, as the increased slot leakage would result in higher AC copper losses, however this is beyond the scope of this paper so has been ignored for now. With the iron losses, copper losses, and machine torque performance evaluated at rated speed the efficiencies could be calculated and a breakdown of these results is given in Table VIII.

TABLE VIII LOSS COMPARISON OF EACH MACHINE

Winding Type	Stator Loss (W)	Rotor Loss (W)	PM Loss (W)	Copper Loss (W)	Efficiency (%)
12s/10p 3-phase	3.72	1.25	0.0738	45.08	77.86
12s/10p dual 3-phase	3.73 **(+0.19%)**	0.665 **(-47.01%)**	0.0727 **(-1.50%)**	45.08	78.88 **(+1.30%)**
24s/10p 3-phase	4.72 **(+26.99%)**	1.21 **(-3.19%)**	0.0188 **(-74.58%)**	44.74	77.02 **(-1.08%)**
24s/10p dual 3-phase	4.50 **(+21.08%)**	1.01 **(-19.78%)**	0.0165 **(-77.69%)**	44.74	77.79 **(-0.10%)**
24s/10p 3-phase star-delta	4.51 **(+21.24%)**	0.805 **(-35.77%)**	0.0157 **(-78.69%)**	44.74	78.44 **(+0.73%)**
24s/10p dual 3-phase star-delta	4.51 **(+21.21%)**	0.790 **(-36.99%)**	0.0152 **(-79.44%)**	44.74	78.63 **(+0.99%)**

The 24-slot machines each exhibits higher stator losses than either of the 12-slot machines, an expected outcome due to the thinner teeth causing higher saturation. The 12-slot dual 3-phase machine has the largest reduction in rotor losses of any of the machines which in turn gives it the highest efficiency. However, it does little to reduce the PM eddy current losses when compared with the conventional 3-phase machine, likely due to its lack of 7th order harmonic reduction. The 24-slot machines each show a reasonable reduction in rotor losses, with the dual 3-phase machine with star-delta winding exhibiting the largest reduction. Each of the 24-slot machines show substantial reduction in PM eddy current losses, again with the dual 3-phase machine with star-delta windings reaching the largest reduction. This culminates in an almost comparable efficiency between the 24-slot dual 3-phase machine with star-delta windings and the 12-slot dual 3-phase machine.

V. Experimental Validation

To validate the simulations in this paper, a 24-slot 10-pole prototype machine with dual star-delta windings was manufactured, as shown in Fig. 15. This machine was then compared against an existing 12s/10p dual 3-phase prototype machine. The specifications for both machine specifications can be found in TABLE I.

(a)

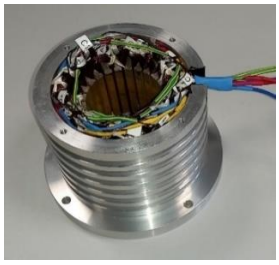

(b)

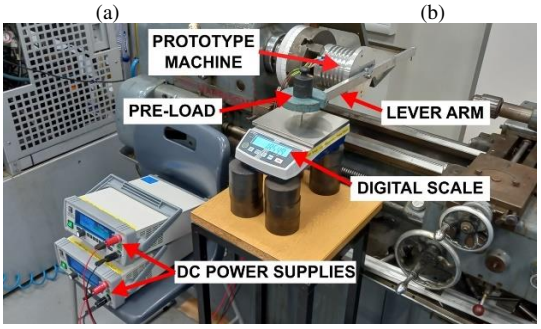

(c)

Fig. 15 Dual star-delta prototype machine. (a) Close up of winding layout, (b) installation in the stator housing and (c) experimental setup.

A. EMF Measurements

Initially the prototype machine was spun at rated speed to measure the EMFs of the individual star and delta coils. For the star coils, the phase EMF was measured, but due to the nature of a delta winding only the line EMF could be measured. The measured waveforms across the star and delta coils are compared with simulated results in Fig. 16. A good agreement can be observed between the simulated and measured results with only a slight reduction in the amplitude of the measured EMF (about 3% for both winding types). It is also found that, unlike the star windings, the 3rd order EMF harmonic circulates within the delta windings, and hence it is not present in the line EMF.

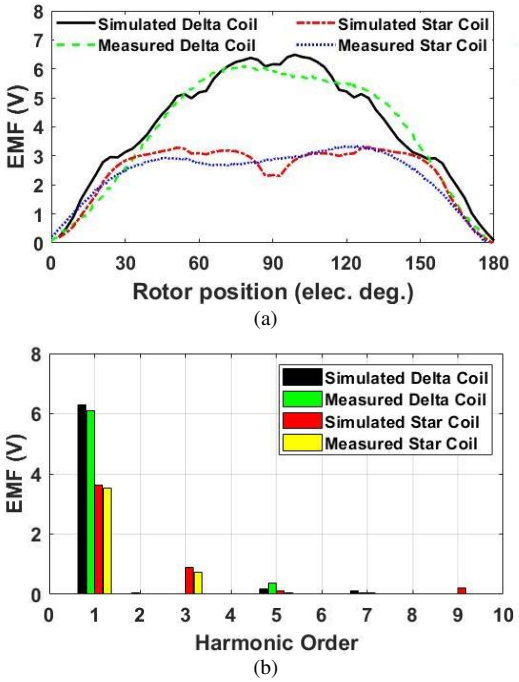

Fig. 16. EMFs of star and delta coils. (a) Waveforms and (b) spectra.

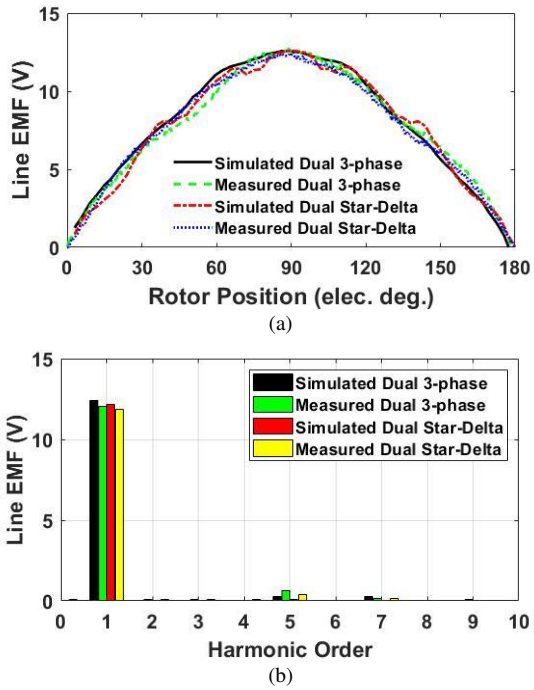

Fig. 17. Line EMF for dual 3-phase and dual star-delta winding machine. (a) Waveform and (b) harmonic comparison.

In addition to the measurement of EMFs of individual star and delta windings, the line EMF of the complete star-delta winding has also been measured and compared against the simulated results, as shown in Fig. 17. Again, considering unavoidable manufacturing tolerance, the agreement between the simulated and measured results is deemed good enough. This has been comparatively plotted against results for a dual 3-phase 12s/10p machine, where there is a minor reduction in the line EMF at this rated speed.

B. Static Torque Measurements

To validate the torque performance of the dual star-delta winding machine, a couple of static torque experiments were carried out using the method detailed in [31]. This method can be used to measure both the cogging torque and the onload torque. However, due to the periodicity of the cogging torque being 3 mech. deg. and the expected amplitude being 0.01Nm, it was not possible to obtain a waveform of cogging torque. The margin for measurement error on the rotor position, coupled with 'noise' that could vary the torque even slightly made obtaining accurate results impossible. However, the static onload torque could be measured. Using two DC power supplies to excite the two 3-phase winding sets in such a way that $I_{A1} = I_{A2} = I$, $I_{B1} = I_{B2} = -I/2$ and $I_{C1} = I_{C2} = -I/2$, where I is the DC current, the static torque of the machine rotated through 360 elec. deg. could be measured, as shown in Fig. 18 (a). Additionally, the peak static torque at 90 elec. deg. phase angle was measured at increasing phase currents, as shown in Fig. 18 (b). Again, there is a close match between the simulated and measured results with only a slight discrepancy under 2%. At higher phase currents, the torque performance of the dual star-delta wound machine begins to outperform that of the dual 3-phase machine, which corroborates the results obtained by FEA.

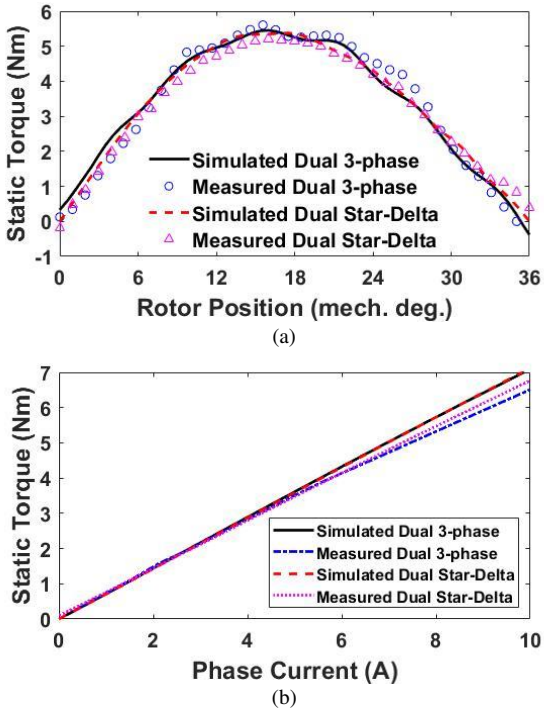

Fig. 18. Measured and simulated static torques. (a) Static torque *vs* current phase angle and (b) peak static torque (at 90 elec. deg.) *vs* increasing phase current.

VI. Conclusion

In this paper a 24s/10p dual 3-phase PM machine with star-delta windings has been proposed to improve machine electromagnetic performance. This has been achieved by combining the principles of stator shifting, operating the

second winding set at a 15 elec. deg, phase shift using a second converter, and implementing star-delta windings on each of the 3-phase sets. The concept has been proved by analytical modelling and FE simulations. For a 24s/10p machine, the star-delta winding can eliminate the 1st order sub-space harmonic, and the second converter successfully eliminates the 7th order super harmonic. Additionally, the 24-slot dual 3-phase star-delta winding achieved the largest increase in working harmonic over a conventional 12-slot 3-phase machine.

FEA results showed that the proposed dual 3-phase machine with star-delta windings could achieve similar or even higher average torque to the 12-slot dual 3-phase machine. Additionally, the dual 3-phase machine with star-delta windings showed a substantial reduction in torque ripple coefficient, 0.99% compared with 6.59% for the 12-slot dual 3-phase machine. It also showed the greatest reduction in PM eddy current losses, this being beneficial in reducing the risk of thermal demagnetization. The combination of low rotor eddy current losses and reduced PM eddy current losses resulted in an overall machine efficiency that was comparable to the 12-slot dual 3-phase machine. A prototype machine was manufactured and both EMF and static torque measurements closely match the simulation results, corroborating the expected performance of the 24-slot 10-pole machine with dual star-delta windings.

ACKNOWLEDGMENT

This work is supported by the UK EPSRC Prosperity Partnership “A New Partnership in Offshore Wind” under Grant No. EP/R004900/1.

REFERENCES

[1] A. M. El-Refaie, "Fractional-Slot Concentrated-Windings Synchronous Permanent Magnet Machines: Opportunities and Challenges," *IEEE Trans. Ind. Electron.,* vol. 57, no. 1, pp. 107-121, Jan. 2010.

[2] N. Bianchi and M. D. Pre, *Use of the star of slots in designing fractional-slot single-layer synchronous motors* (Proc. Inst. Elect. Eng.—Electr. Power Appl). 2006.

[3] A. M. El-Refaie, T. M. Jahns, and D. W. Novotny, "Analysis of Surface Permanent Magnet Machines With Fractional-Slot Concentrated Windings," *IEEE Trans. Energy Convers.,* vol. 21, no. 1, pp. 34-43, Mar. 2006.

[4] A. M. El-Refaie, Z. Q. Zhu, T. M. Jahns, and D. Howe, "Winding Inductances of Fractional Slot Surface-Mounted Permanent Magnet Brushless Machines," in *2008 IEEE Industry Applications Society Annual Meeting*, Edmonton, Alberta, Canada, Oct. 2008.

[5] N. Bianchi, S. Bolognani, M. D. Pre, and G. Grezzani, "Design considerations for fractional-slot winding configurations of synchronous machines," *IEEE Trans. Ind Appl,* vol. 42, no. 4, pp. 997-1006, July 2006.

[6] D. Ishak, Z. Q. Zhu, and D. Howe, "Comparative study of permanent magnet brushless motors with all teeth and alternative teeth windings," presented at the Second IEE International Conference on Power Electronics, Machines and Drives, Edinburgh, UK, Mar., 2004.

[7] D. Ishak, Z. Q. Zhu, and D. Howe, "Analytical prediction of rotor eddy current losses in permanent magnet brushless machines with all teeth and alternate teeth windings—Part I: Polar co-ordinate model," presented at the ICEMS, Lodz, Poland, Sept., 2004.

[8] Z. Q. Z. D. Ishak, and D. Howe, "Analytical prediction of rotor eddy current losses in permanent magnet brushless machines with all teeth and alternate teeth windings—Part II: Rectangular co-ordinate model," presented at the ICEMS, Lodz, Poland, Sept., 2004.

[9] D. Ishak, Z. Q. Zhu, and D. Howe, "Comparison of PM Brushless Motors, Having Either All Teeth or Alternate Teeth Wound," *IEEE Trans. Energy Convers.,* vol. 21, no. 1, pp. 95-103, Mar. 2006.

[10] K. Atallah, D. Howe, P. H. Mellor, and D. A. Stone, "Rotor loss in permanent magnet brushless AC machines," in *IEEE International Electric Machines and Drives Conference. IEMDC'99. Proceedings (Cat. No.99EX272)*, 1999: IEEE.

[11] N. Bianchi, S. Bolognani, and E. Fomasiero, "A General Approach to Determine the Rotor Losses in Three-Phase Fractional-Slot PM Machines," in *2007 IEEE International Electric Machines & Drives Conference*, May 2007: IEEE.

[12] N. Bianchi and E. Fornasiero, "Impact of MMF Space Harmonic on Rotor Losses in Fractional-Slot Permanent-Magnet Machines," *IEEE Trans. Energy Convers.,* vol. 24, no. 2, pp. 323-328, June 2009.

[13] N. Yogal, C. Lehrmann, and M. Henke, "Measurement of eddy current loss in permanent magnets with high-frequency effects of electrical machines for hazardous locations," in *2019 22nd International Conference on Electrical Machines and Systems (ICEMS)*, Aug. 2019: IEEE.

[14] M. Nakano, H. Kometani, and M. Kawamura, "A study on eddy-current losses in rotors of surface permanent-magnet synchronous machines," *IEEE Trans. Ind Appl,* vol. 42, no. 2, pp. 429-435, Mar. 2006.

[15] G. Dajaku, W. Xie, and D. Gerling, "Reduction of Low Space Harmonics for the Fractional Slot Concentrated Windings Using a Novel Stator Design," *IEEE Trans. Magn.,* vol. 50, no. 5, pp. 1-12, May 2014.

[16] P. B. Reddy, A. M. El-Refaie, and K.-K. Huh, "Effect of number of layers on performance of fractional-slot concentrated-windings interior permanent magnet machines," in *8th International Conference on Power Electronics - ECCE Asia*, May 2011: IEEE.

[17] G. Dajaku and D. Gerling, "A Novel 24-Slots/10-Poles Winding Topology for Electric Machines," in *2011 IEEE International Electric Machines & Drives Conference (IEMDC)*, Ontario, Canada, May 2011.

[18] P. B. Reddy, K.-K. Huh, and A. M. El-Refaie, "Generalized Approach of Stator Shifting in Interior Permanent-Magnet Machines Equipped With Fractional-Slot Concentrated Windings," *IEEE Trans. Ind. Electron.,* vol. 61, no. 9, pp. 5035-5046, Sept. 2014.

[19] A. S. Abdel-Khalik, S. Ahmed, and A. M. Massoud, "A Six-Phase 24-Slot/10-Pole Permanent-Magnet Machine With Low Space Harmonics for Electric Vehicle Applications," *IEEE Trans. Magn.,* vol. 52, no. 6, pp. 1-10, June 2016.

[20] A. M. El-Refaie, M. R. Shah, R. Qu, and J. M. Kern, "Effect of Number of Phases on Losses in Conducting Sleeves of Surface PM Machine Rotors Equipped With Fractional-Slot Concentrated Windings," *IEEE Trans. Ind Appl,* vol. 44, no. 5, pp. 1522-1532, Sept. 2008.

[21] N. Bianchi, M. D. Pre, G. Grezzani, and S. Bolognani, "Design considerations on fractional-slot fault-tolerant synchronous motors," in *IEEE International Conference on Electric Machines and Drives, 2005.*, Jan. 2005: IEEE.

[22] N. Bianchi, S. Bolognani, and M. Dai Pre, "Design and Tests of a Fault-Tolerant Five-phase Permanent Magnet Motor," in *37th IEEE Power Electronics Specialists Conference*, 2006: IEEE.

[23] N. Bianchi, S. Bolognani, and M. Dai Pre, "Strategies for the Fault-Tolerant Current Control of a Five-Phase Permanent-Magnet Motor," *IEEE Trans. Ind Appl,* vol. 43, no. 4, pp. 960-970, Jan. 2007.

[24] X. Chen, J. Wang, V. I. Patel, and P. Lazari, "A Nine-Phase 18-Slot 14-Pole Interior Permanent Magnet Machine With Low Space Harmonics for Electric Vehicle Applications," *IEEE Trans. Energy Convers.,* vol. 31, no. 3, pp. 860-871, Sept. 2016.

[25] M. Barcaro, N. Bianchi, and F. Magnussen, "Analysis and tests of a dual three-phase 12-slot 10-pole permanent magnet motor," in *2009 IEEE Energy Conversion Congress and Exposition*, Sept. 2009: IEEE.

[26] M. Barcaro, N. Bianchi, and F. Magnussen, "Six-Phase Supply Feasibility Using a PM Fractional-Slot Dual Winding Machine," *IEEE Trans. Ind Appl,* vol. 47, no. 5, pp. 2042-2050, Sept. 2011.

[27] A. S. Abdel-Khalik, S. Ahmed, and A. M. Massoud, "Low Space Harmonics Cancelation in Double-Layer Fractional Slot Winding Using Dual Multiphase Winding," *IEEE Trans. Magn.,* vol. 51, no. 5, pp. 1-10, May 2015.

[28] M. S. Islam, M. A. Kabir, R. Mikail, and I. Husain, "Space-Shifted Wye–Delta Winding to Minimize Space Harmonics of Fractional-Slot Winding," *IEEE Trans. Ind Appl,* vol. 56, no. 3, May 2020.

[29] G.-J. Li, Z.-Q. Zhu, M. P. Foster, D. A. Stone, and H.-L. Zhan, "Modular Permanent-Magnet Machines With Alternate Teeth Having Tooth Tips," *IEEE Trans. Ind. Electron.,* vol. 62, no. 10, pp. 6120-6130, Oct. 2015.

[30] A. Tessarolo, M. Mezzarobba, and M. Degano, "Analytical calculation of air-gap armature reaction field including slotting effects in fractional-slot concentrated-coil SPM multiphase machines," in *2011 International Conference on Power Engineering, Energy and Electrical Drives*, Malaga, Spain, May 2011.

[31] Z. Q. Zhu, "A simple method for measuring cogging torque in permanent magnet machines," in *IEEE Power & Energy Society General Meeting*, July 2009: IEEE.